ACS APPLIED MATERIALS & INTERFACES

Research Article

www.acsami.org

Preparation and Release Behavior of Chlorpyrifos Adsolubilized into Layered Zinc Hydroxide Nitrate Intercalated with Dodecylbenzenesulfonate

Jiexiang Liu,[†] Xiaoguang Zhang,*[,‡] and Yongqing Zhang[†]

[†]School of Chemical Engineering, Hebei University of Technology, Tianjin 300130, P. R. China

[‡]College of Chemistry, Nankai University, Tianjin 300071, P. R. China

Supporting Information

ABSTRACT: A novel method was developed to make the charge-neutral and poorly water-soluble pesticide chlorpyrifos (CPF) adsolubilize into layered zinc hydroxide nitrate intercalated with dodecylbenzenesulfonate (ZHN-DBS). It included two steps: first, CPF was solubilized into the micelles formed by anionic surfactant sodium dodecylbenzenesulfonate (DBS), nonionic surfactant polyoxyethylene (10) nonyl phenyl ether (TX-10) or zwitterionic surfactant dodecyl betaine (DB), and then ZHN−DBS was poured into CPF micelles to synthesize ZHN−DBS−CPF, ZHN−TX-10−CPF, and ZHN−DB−CPF intercalated compounds. These intercalated compounds were characterized by powder X-ray diffraction (XRD), Fourier transform infrared spectroscopy (FT-IR), and thermogravimetric analysis and differential thermal analysis (TGA/DTA). The results showed that ZHN−DBS−CPF, ZHN−TX-10−CPF, and ZHN−DB−CPF had the basal spacings of 3.29−3.59, 2.57−2.87, and 1.97 nm, respectively, which was discussed from the intercalated mechanism. The intercalated CPF had the higher thermal stability. Release behaviors of CPF from intercalated compounds were investigated and analyzed in buffer solutions (pH 5.0 and 6.8). The results exhibited that the release rates and equilibrium release amounts of CPF were closely dependent on micelles types and release mediums. The release behaviors of ZHN−DBS−CPF and ZHN−TX-10−CPF were well described with pseudo second-order and parabolic diffusion models. The present study suggested that ZHN−DBS−CPF and ZHN−TX-10−CPF could be applied as a potential pesticide delivery system.

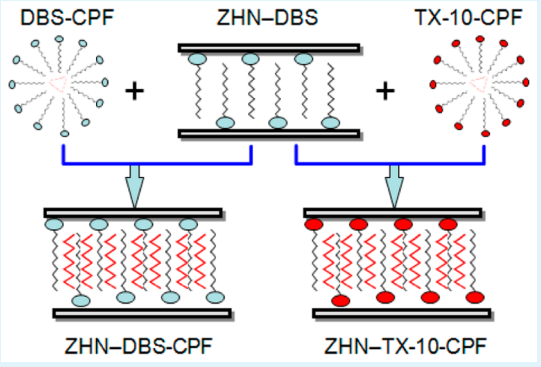

KEYWORDS: *layered zinc hydroxide nitrate (ZHN), chlorpyrifos, micelle, surfactant, release behavior*

1. INTRODUCTION

Layered metal hydroxides can typically be classified into layered double hydroxides (LDH) and layered hydroxide salts (LHS). Both LDH and LHS are modifications of the brucite-like structure. The brucite structure is based on individual layers of Mg^{2+}-centered octahedra with OH^- located in the vertices. Each OH^- is surrounded by three metal cations to result in neutral layer.[1] The brucite structure can undergo compositional changes when a trivalent cation of M^{3+} isomorphically replaces part of Mg^{2+}, forming an excess of charge in the layer that must be neutralized by interlayer anions. These modifications cause a series of compounds called LDH with the general formula $M^{2+}_{1-x}M^{3+}_{x}(OH)_2(A^{m-})_{x/m}\cdot nH_2O$, where the M^{n+} are metal cations (M^{2+} =Mg^{2+}, Ni^{2+}, Zn^{2+}, Cu^{2+}, ..., M^{3+} = Al^{3+}, Fe^{3+}, ...) and A^{m-} are interlayer anions (A^{m-} = CO_3^{2-}, NO_3^-, SO_4^{2-}, and other anionic species).[2] These interlayer anions can be replaced by a wide range of functional anions through the ion-exchange process.[3] As a result LDH have been widely explored as hosts for flame retardancy,[4,5] the storage and controlled release of a spectrum of functional guests.[6−9] Brucite-like structures can experience other modifications, but instead of the metal replacement, hydroxide ions are removed from the structure and replaced by water molecules or other types of oxoanions to balance the charge of the layers. These modifications lead to a type of compounds called LHS represented by the general formula $M^{2+}(OH)_{2-x}(A^{m-})_{x/m}\cdot nH_2O$, in which M^{2+} is one or two types of metallic cations, such as Cu^{2+}, Co^{2+}, Ni^{2+}, or Zn^{2+}, and A^{m-} is the exchangeable anion. LHS has the similar anion-exchange properties as LDH. LHS shows much more promising. This is because a single metal ion presents in the O_h sites and it has the ability to partly exchange the hydroxyl groups for larger anions. However, the intercalation chemistry of LHS has received little attention in the past decades of years.[10] In recent years, a large number of studies about LHS have been reported in different application fields, such as drug delivery systems,[11] colored fillers,[12] ultraviolet ray absorbers,[13] as well as they have specific magnetic[14] and catalytic properties.[15,16]

Received: February 3, 2015
Accepted: May 13, 2015
Published: May 13, 2015

DOI: 10.1021/acsami.5b01068
ACS Appl. Mater. Interfaces 2015, 7, 11180−11188

Among the LHS, layered zinc hydroxide nitrate (ZHN) with the formula $Zn_5(OH)_8(NO_3)_2{\cdot}2H_2O$ has been the most subject studied as intercalation matrix. ZHN is formed by a layer with octahedral coordinated zinc cations in which one-quarter are displaced, leaving an empty octahedral site, and forming cationic centers tetrahedrically coordinated up and down to the octahedral sheet. The tetrahedron apex is occupied by a water molecule and the nitrate ions are free in the interlayer.[17] ZHN material is particularly well suited for use in biomedical and agricultural fields because of its high biocompatibility. ZHN intercalation compounds have exhibited the different behaviors compared to LDH. ZHN modified with carboxylic acids is more prone to undergo functionalization than that of ZnAl−LDH.[18] The aspartic acid intercalated into ZHN has presented higher thermal stability than that of LDH.[19] The indole-3-acetic acid (IAA) release from ZHN is slower than LDH because the IAA interaction with the ZHN lattice is much stronger than LDH.[11] The caffeic acid (CA) intercalated into ZHN has exhibited a superior UV screening ability compared to pure CA molecule.[20] The p-coumaric acid (pCA) intercalated into ZHN has shown the comparable antioxidant activity to the free pCA.[21]

Synthesis of pesticide intercalation compounds have been developed by many methods, such as coprecipitation,[22] ion exchange,[23] and reconstruction.[24] To the best of our knowledge, the majority of literatures on these methods are limited to the anionic pesticides. However, for charge-neutral and poorly water-soluble pesticides, their intercalation is usually dependent on anionic surfactant that forms a hydrophobic region in the gallery.[25,26] The hydrophobic nature and accessibility of the interlayer region of LDH is helpful for adsorption of target pesticide molecules,[27−30] showed in Scheme 1a. Moreover,

Scheme 1. Preparation Methods of Intercalated Compounds
P: pesticide; S: surfactant; LHS: layered hydroxide salts

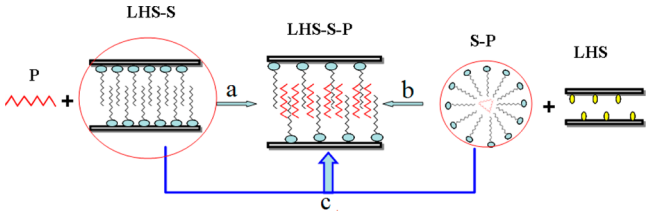

Tyner et al.[31] have developed a novel method to synthesize camptothecin−LDH intercalated compounds. Camptothecin has been first incorporated into micelles derived from anionic surfactants, and then the micelles were introduced to the galleries of MgAl−LDH, shown in Scheme 1b. The similar method has also been adopted by Quan et al.[32] to synthesize bactericides (hexaconazole and triadimenol)−LDH intercalated compounds. Nonionic hydrophobic pesticide chlorpyrifos (CPF) has been intercalated into LDH−dodecylsulfonate (LDH−DSO) and LDH−DBS[29] by Scheme 1a. However, the CPF loaded content has been only 1.3−1.4% for LDH−DSO and 2.9−3.1% for LDH−DBS, respectively. In this study, we have tried to incorporate CPF into the gallery of ZHN by the methods in Scheme 1a and b. However, the sample prepared by Scheme 1a has the smaller basal spacing than the pristine ZHN−DBS and CPF release is comparably rapid. The sample prepared by Scheme 1b displays a very weak peak at low angle. These indicate that CPF has not been effectively intercalated into the gallery. Therefore, we have developed a novel method to make CPF adsolubilize into the interlayer of ZHN intercalated with dodecylbenzenesulfonate (DBS). First, ZHN is modified with DBS to form a hydrophobic region in the gallery of ZHN−DBS; then, CPF is solubilized into the micelles derived from DBS, TX-10, or DB, respectively; finally, ZHN−DBS is mixed with CPF micelles to prepare the CPF intercalated compounds (Scheme 1c). The release behaviors of ZHN−DBS−CPF, ZHN−TX-10−CPF, and ZHN−DB−CPF are investigated. The results show that the CPF loading is greatly increased and the samples display the improved release behavior. ZHN−DBS−CPF and ZHN−TX-10−CPF are the potential controlled-release formulation of pesticide. Furthermore, the CPF release mechanism of ZHN−DBS−CPF and ZHN−TX-10−CPF is also analyzed based on three kinetic models.

2. EXPERIMENTAL SECTION

2.1. Materials. Sodium dodecylbenzenesulfonate (DBS) was purchased from China Pharmacy Shanghai Chemical Co., China, polyoxyethylene (10) nonyl phenyl ether (TX-10) from Jilian Petroleum Chemistry Co., Ltd., China. Dodecyl betaine (DB) was purchased from China Research Institute of Daily Chemical Industry and was purified by extraction with petroleum ether and recrystallization from acetone for three times, respectively. Chlorpyrifos (CPF) from Shandong Zhanhua Tianyuan Fine Chemical Co., Ltd., China. NaOH are of analytical grade from North Tianjin Pharmacy Chemical Reagent, China, $Zn(NO_3)_2{\cdot}6H_2O$ are of analytical grade from Tianjin Kemiou Chemical Co., Ltd., China. Decarbonated deionized water is used throughout the experiments.

2.2. Synthesis. Layered zinc hydroxide nitrate (ZHN) was synthesized by following a procedure described elsewhere.[13,33] In short, ZHN was prepared by the slow addition of 1.0 mol·L^{-1} NaOH into 40 mL of solution containing 0.5 mol·L^{-1} of Zn $(NO_3)_2{\cdot}6H_2O$, under magnetic stirring, with the final pH values adjusted to around 6.5. The obtained slurry was magnetically stirred at 30 °C for 24 h under a nitrogen atmosphere. The solid was filtered, followed by washing with decarbonated water. The process was repeated three times. The final white solid, labeled as ZHN, was dried in an oven overnight at 80 °C.

Preparation of DBS intercalated into the gallery of ZHN (denoted as ZHN−DBS) was carried out by coprecipitation method. Twenty ml of 0.5 mol·L^{-1} Zn $(NO_3)_2{\cdot}6H_2O$ solution and 18 mL of 0.5 mol·L^{-1} NaOH were synchronously added into 20 mL of 0.23 mol·L^{-1} DBS solution under a nitrogen atmosphere. The pH value was controlled at around 6.5. After precipitation, the mixture was kept for 0.5 h under the same condition, and then transferred into Teflon-lined stainless-steel autoclave and maintained at 60−100 °C for 3 h. After the hydrothermal treatment, the mixture was filtered, followed by washing three times with the decarbonated water. The final white solid was dried in an oven overnight at 80 °C.

ZHN−DBS−CPF, ZHN−TX-10−CPF, and ZHN−DB−CPF were synthesized and described as follows: CPF was dissolved in alcohol, and was added to the certain concentration DBS (TX-10 or DB) solution, denoted as DBS-CPF (TX-10-CPF or DB-CPF) micelles. 0.8 g of ZHN−DBS was then added into the micelles and stirred under N_2 at 30 °C for 48 h. The mixture was filtered and washed several times with deionized water and alcohol. The final solid was dried in an oven overnight at 60 °C, denoted as ZHN−DBS−CPF (m, n), ZHN−TX-10−CPF (m, n), and ZHN−DB−CPF (m, n), in which the m and n indicated the mass of DBS (TX-10) and CPF in micelles, respectively. In addition, for making comparison, we tried to prepare CPF intercalation into ZHN by other two methods: one method was that ZHN was added into DBS-CPF micelles and stirred 30 °C for 48 h, the final solid denoted as ZHN−DBS−CPF-1; the other was that ZHN−DBS was mixed into CPF alcohol solution and stirred at 30 °C for 48 h, the final solid denoted as ZHN−DBS−CPF-2.

2.3. Characterization. Powder X-ray diffraction diagrams (XRD) were performed on D8 Foucas using Ni filtered Cu Kα radiation (λ =

DOI: 10.1021/acsami.5b01068
ACS Appl. Mater. Interfaces 2015, 7, 11180−11188

1.54056 Å). XRD experiments were performed in the range of 2θ between 2 and 80° generated at 40 kV and 40 mA at room temperature. FT-IR spectra (4000−400 cm^{-1}) were recorded on a Vector 22 (Bruker, Germany) Fourier transform infrared spectrometer using the KBr disk method with a ratio sample/KBr of 1:100 by mass. Elemental analysis was performed by inductively coupled plasma (ICP) emission spectroscopy on an IRIS Advantage (Thermo, USA) for Zn analysis after dissolving the samples in HCl solution. Elemental analysis of C, H, N were performed in vario EL CUBE (Elementar, Germany). Elemental analysis of Cl was performed by ion chromatograph (Thermo Electron, USA). Thermogravimetric analysis and differential thermal analysis (TGA/DTA) measurements were performed in SDT Q600 synchronization thermoanalyzer (IA company, USA) in air at a heating rate of 10 °C/min, in the range 20−800 °C. UV−vis absorption spectra were recorded on TU1221 spectrophotometer.

2.4. Release Studies. *2.4.1. Determination of CPF Loading.* The loaded amount of CPF in ZHN−DBS−CPF (ZHN−TX-10−CPF or ZHN−DB−CPF) was determined by UV−vis spectroscopy. A known weight of ZHN−DBS−CPF (ZHN−TX-10−CPF or ZHN−DB−CPF) sample was placed in a 10 mL volumetric test tube. A moderate volume of 1 mol·L^{-1} HCl was added to dissolve the inorganic layers and then ethanol was used to fill the balance. Then the concentration of CPF in solution was determined by monitoring the absorbance at λ_{max} = 300.5 nm, and the concentration was calculated by regression analysis according to the standard curve obtained from a series of standard solution of CPF. The final value was an average of measurements of three parallel samples. The amount of loaded CPF was obtained according to the concentration of CPF in the solution and the mass of ZHN-DBS-CPF (ZHN−TX-10−CPF or ZHN−DB−CPF) sample used.

2.4.2. Determination of Release Behavior. ZHN−DBS−CPF (0.02 g; 0.01 g of ZHN−TX-10−CPF or ZHN−DB−CPF) intercalated compounds sample was dispersed in 250 mL buffer solution at pH 5.0 and 6.8 under magnetic stirring at 30 °C. The buffer solutions at pH 5.0 and 6.8 were achieved by the phosphate solutions. Three ml of supernatant were withdrawn at different times and replaced by the same amount of fresh medium. The withdrawn supernatant were filtered, and their CPF contents were determined by monitoring the absorbance at λ_{max} = 300.5 nm to obtain the release amounts of CPF, in turn to calculate the accumulated percent releases of CPF from the intercalated compounds. Release tests were performed repeatedly for three times and the results were recorded as an average. The standard error of release experiment is <3.0%.

2.4.3. Release Kinetics Models. To understand the release mechanisms of CPF from ZHN−DBS−CPF and ZHN−TX-10−CPF, the release data were fitted by three kinetic models:[11,34,35]

The first-order model describes the drug release process where the dissolution depends on the drug loading in intercalated compounds and can be expressed as

$$-\ln(1 - x_t) = k_1 t \quad (1)$$

The pseudo-second-order model has been applied to describe the influencing factors of adsorption (such as liquid film diffusion, surface adsorption, particle inner diffusion) or describe release kinetic process. The equation is generally described as

$$\frac{t}{x_t} = \frac{1}{k_2 q_e} + t \quad (2)$$

The parabolic diffusion model describes diffusion-controlled process in clays, and the equation is as follows:

$$\frac{x_t}{t} = k_p t^{-0.5} + m \quad (3)$$

In above equation, where x_t is the release percentage at any time (t), k_1 (k_2 or k_p) is the corresponding rate constant of release kinetics. If the release kinetics is applicable, the plot of $\ln(1 - x_t)$ versus t (t/x_t vs t, x_t/t vs $t^{-0.5}$) will be linear, and the k value can be obtained from the slope of the linear plot.

3. RESULTS AND DISCUSSION

3.1. Characterization of the Pristine ZHN−DBS, ZHN−DBS−CPF, ZHN−TX-10−CPF, and ZHN−DB−CPF.

3.1.1. XRD Analysis. XRD patterns of a series of ZHN−DBS with different DBS concentrations (0.019−0.38 mol·L^{-1}) are displayed in Figure 1. Figure 1a presents XRD pattern of ZHN,

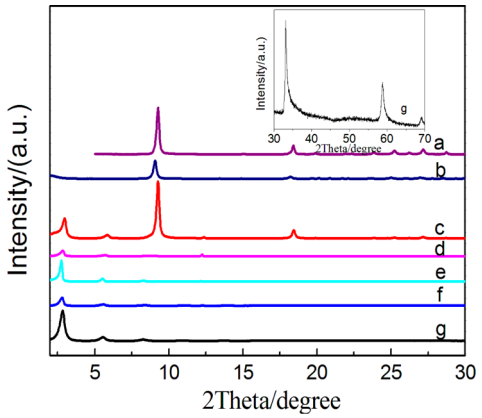

Figure 1. XRD patterns of a series of ZHN−DBS with different DBS concentrations; the figure inset for *g* sample magnification at 2θ = 30−70°: (a) 0, (b) 0.019, (c) 0.096, (d) 0.19, (e) 0.23, (f) 0.30, (g) 0.38 mol·L^{-1}.

which corresponds to the previously published data [JCPDS-PDF 24-1460] .[36,37] The first diffraction peak at 9.1° corresponds to the basal spacing of 0.95 nm allowing NO_3^- to adopt an approximately perpendicular orientation to the layers. The sample is well crystallized without impurities such as ZnO. Moreover, the basal spacing of ZHN is about 0.1 nm higher than that of LDH due to tetrahedral Zn atoms protruded into the interlayer.[38] As DBS concentration is 0.019 mol·L^{-1}, the sample still displays the typical ZHN pattern (Figure 1b), and the diffraction intensity decreases apparently and the basal spacing widens slightly to 0.98 nm. When DBS concentration is increased to 0.096 mol·L^{-1}, a new lamellar structure attributed to ZHN−DBS is distinctly observed in Figure 1c. Its diffraction peak located at 2.8° corresponds to the basal spacing of 3.15 nm, suggesting DBS intercalation into the galleries. When DBS concentration is in the range of 0.19−0.38 mol·L^{-1}, samples only display the typical ZHN−DBS structure without impurities such as ZnO and ZHN. The interlayer space available for intercalated DBS can be estimated by subtracting a thickness of the hydroxide layer (i.e., 0.48 nm) and two zinc tetrahedron (0.26 × 2 nm) from the basal spacing. The obtained gallery height of about 2.15 nm is comparable with the size of DBS molecule along the long axis (1.90 nm[32]). This suggests that DBS forms a tilt monolayer in the gallery when the SO_3 group approaches the layer by three oxygen atoms, which is different from that in LDH.[29,39] Nonbasal diffractions located around 33°, 58°, and 69°confirm the identity of the hydroxide layers (Figure 1 inset). Moreover, with increasing DBS concentration, the sample presents a colloid state appearance probably because of an excess of DBS adsorbed on the surface. Therefore, 0.23 mol·L^{-1} DBS is selected as an optimum to further synthesize samples in the following sections. On the basis of this, ZHN−DBS is prepared at pH = 6.0, 6.5, and 7.0, respectively. All samples display a typical ZHN−DBS pure phase, and the good crystallinity is observed for the sample prepared at pH 6.5 (Supporting Information

DOI: 10.1021/acsami.5b01068
ACS Appl. Mater. Interfaces 2015, 7, 11180−11188

Figure S1A). In addition, the slurry prepared at pH 6.5 is hydrothermally treated at 60, 80, and 100 °C, respectively. These samples display the typical ZHN−DBS pure phase (Supporting Information Figure S1B). Therefore, 0.23 mol·L^{-1} DBS, pH 6.5, and hydrothermal temperature at 60 °C for 3h are selected as an optimal condition to synthesize ZHN−DBS.

On the basis of the above, ZHN-DBS is poured into CPF micelle formed by anionic surfactant DBS, nonionic surfactant TX-10 and zwitterionic surfactant DB to synthesize ZHN−DBS−CPF, ZHN−TX-10−CPF, and ZHN−DB−CPF intercalated compounds, respectively. Figure 2 displays XRD

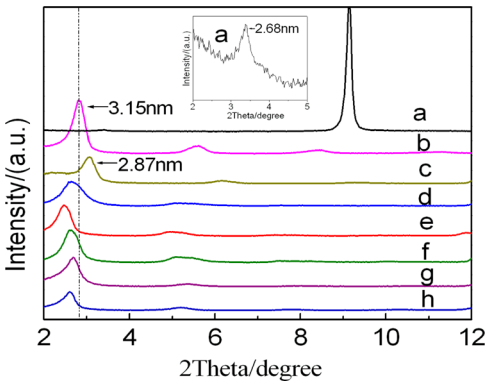

Figure 2. XRD patterns of ZHN−DBS−CPF samples; the figure inset for *a* sample magnification at $2\theta < 5°$: (a) ZHN−DBS−CPF-1, (b) ZHN−DBS, (c) ZHN−DBS−CPF-2, (d) ZHN−DBS−CPF (1.2, 1.2), (e) ZHN−DBS−CPF (1.2, 0.6), (f) ZHN−DBS−CPF (1.2, 1.0), (g) ZHN−DBS−CPF (0.6, 1.0), (h) ZHN−DBS−CPF (1.5, 1.0).

patterns of a series of ZHN−DBS−CPF (*m*, *n*). The first diffraction peak positions are in the range of 2.5−2.7°. Their basal spacings are widened to 3.29−3.59 nm compared to that of ZHN−DBS (3.15 nm), indicating the successful CPF incorporation into the gallery. However, for ZHN−DBS−CPF-1 (see in the Experimental Section), a very weak peak detected at 3.3° (Figure 2 inset) attributes to the intercalation of DBS and CPF molecules, and a strong peak at 9.1° corresponds to ZHN structure. This indicates DBS-CPF micelle cannot be effectively intercalated into the interlayer because of the weak driving force. For ZHN−DBS−CPF-2 (see in the Experimental Section), the basal spacing is 2.87 nm and samller than that of ZHN−DBS. This may be due to that part of DBS molecules remove from the interlayer and form the DBS-CPF micelles in the solution. Compared to ZHN−DBS−CPF-1 and ZHN−DBS−CPF-2, ZHN−DBS−CPF may be the result of two synergistic effects: on one hand, ZHN−DBS provides the hydrophobic region, which benefits the intercalation of DBS−CPF micelles into the gallery; on the other hand, the attractive interaction between DBS−CPF micelles and layer further promotes the DBS−CPF intercalation. Therefore, the CPF incorporation into ZHN−DBS−CPF can be well achieved by the second intercalation of DBS−CPF micelles into the enlarged gallery of ZHN−DBS (Scheme 2).

Figure 3 represents XRD patterns of a series of ZHN−TX-10−CPF. The first diffraction peak positions are in the range of 3.1−3.4°. The corresponding basal spacings are shortened to 2.57−2.87 nm compared to ZHN−DBS. To better explore it, ZHN−TX-10 is also synthesized by the coprecipitation method and XRD pattern is shown in Figure 3a. The very weak peak at 3.3° can be observed because of the weak interaction between TX-10 and the layer. The corresponding basal spacing is 2.65

Scheme 2. Intercalation Mechanism of ZHN−DBS−CPF and ZHN−TX-10−CPF

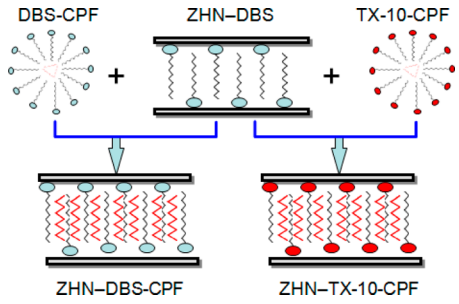

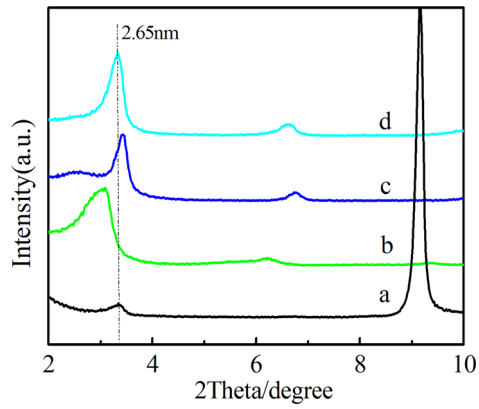

Figure 3. XRD patterns of ZHN−TX-10−CPF samples: (a) ZHN−TX-10, (b) ZHN−TX-10−CPF (0.8, 1.0), (c) ZHN−TX-10−CPF (1.0, 1.0); and (d) ZHN−TX-10−CPF (1.5, 1.0).

nm. It is interesting to find that the basal spacing of ZHN−TX-10−CPF is nearly equal to that of ZHN−TX-10. Furthermore, XRD pattern of the representative ZHN−DB−CPF is displayed in Supporting Information Figure S2. The first diffraction peak position is 4.4°, and the *d*-spacing value is shortened to 1.97 nm.

To further understand their intercalated mechanisms, UV−vis spectra of ZHN−DBS−CPF, ZHN−TX-10−CPF, and ZHN−DB−CPF are showed in Figure 4. The characteristic

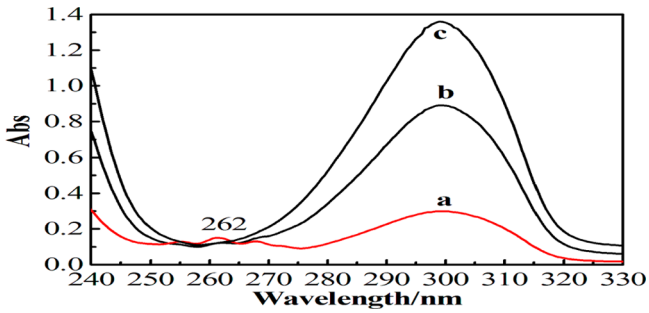

Figure 4. Representative UV−vis spectra curves of CPF loading amount of ZHN−DBS−CPF (a), ZHN−TX-10−CPF (b), and ZHN−DB−CPF (c).

absorption peaks (255, 262, and 268 nm) of DBS are apparently observed in ZHN−DBS−CPF, while it is nearly undetected in ZHN−TX-10−CPF and ZHN−DB−CPF. Combining Figures 4 and 3 (Supporting Information Figure S2), it is further deduced that TX-10 (DB) molecules replace most of DBS during the ZHN−TX-10−CPF (ZHN−DB−

DOI: 10.1021/acsami.5b01068
ACS Appl. Mater. Interfaces 2015, 7, 11180−11188

CPF) preparation. The successful intercalation of TX-10−CPF micells is correlated with the physicochemical properties of TX-10. TX-10 can form the micelles and bring some negative charges due to that it is a nonionic surfactant containing many CH_2CH_2O groups.[40] Thus, it can be intercalated into the gallery via the electrostatic interaction between TX-10 molecules and the layer, and replace most of DBS molecules. In addition, there exists the weak repulsive action among the TX-10 molecules, which makes surfactant molecules close arrangement in the interlayer and CPF molecules locate among TX-10 molecules. This similar phenomenon has been found in the intercalation of 1,5,7-triazabicyclo[4.4.0]dec-5-ene (TBD) into LDH.[41] During ZHN−DB−CPF preparation process, the intercalated DBS is induced and removed from the gallery due to the strong interaction between DB and DBS anions,[42] and the other DB accompanying CPF enter into the gallery through the electrostatic interaction between DB and the layer.

3.1.2. FT-IR Analysis. The CPF molecules incorporated into the interlayer are further confirmed by the FT-IR analysis. Figure 5 displays FT-IR spectra of ZHN, ZHN−DBS, CPF, ZHN−DBS−CPF, and ZHN−TX-10−CPF. For ZHN in Figure 5a, the broad band around 3487 cm^{-1} is attributed to the stretching vibration of the hydroxyl groups in the layers and interlayer water molecules, and a sharp peak at 3579 cm^{-1} causes from the hydroxyl groups belonging to the inorganic lattice, having well-defined vibrational energy.[13] The bending mode of water molecules belongs to the weak band at 1640 cm^{-1}. The sharp peak at 1375 cm^{-1} belongs to the stretching vibration of NO_3^- ions intercalated in the interlayer, similarly to that observed for LDH.[28] For ZHN−DBS in Figure 5b, DBS intercalation is further evidenced by the occurrence of new peak: the bands appeared at 2957, 2926, and 2855 cm^{-1} are assigned to the C−H stretching mode of the alkyl chain; the bands at 1600−1400 cm^{-1} are attributed to backbone vibration of the benzene ring; the bands at 1181 and 1131 cm^{-1} are attributed to the antisymmetrical and symmetrical stretching vibrations of S═O, respectively,[32] indicating the existence of sulfonate; the bands at 1043 and 1012 cm^{-1} come from the C−H vibration of the benzene; the band at 833 cm^{-1} comes from the stretching vibration of S−O. In addition, no characteristic bands of NO_3^- appear in ZHN−DBS. For CPF in Figure 5c, the band around 1551 and 1412 cm^{-1} can be attributed to C═N and C═C stretching modes of the pyridine ring, respectively. The bands at 1167 and 1023 cm^{-1} are due to the stretching vibration of P−O−C of aromatic and aliphatic family, respectively. The band around 852 cm^{-1} can be attributed to P═S stretching modes. The band at 969 cm^{-1} attributes to C−N stretching modes of the pyridine ring. For ZHN−DBS−CPF and ZHN−TX-10−CPF in Figure 5d and 5e, the presence of CPF in the matrix is further evidenced by the occurrence of the characteristic peaks of the pyridine ring located at about 1551, 1412, and 954 cm^{-1}, which is confirmed by UV−vis spectra analysis on characteristic absorption peaks of CPF in Figure 4. Moreover, the characteristic antisymmetrical vibration mode of C−O−C of TX-10 is presented at 1075 cm^{-1}. The FT-IR spectrum of ZHN−DB−CPF is provided in Supporting Information Figure S3. The presence of CPF is further evidenced by the occurrence of the characteristic peaks of the pyridine ring located at about 1523, 1396, and 891 cm^{-1}. Furthermore, the bands at about 2958, 2928, and 2862 cm^{-1} are assigned to the stretching vibration of C−H in the alkyl chain of DB; the peaks at 1590 and 1464 cm^{-1} are attributed to antisymmetric and symmetric peak of C═O, respectively.

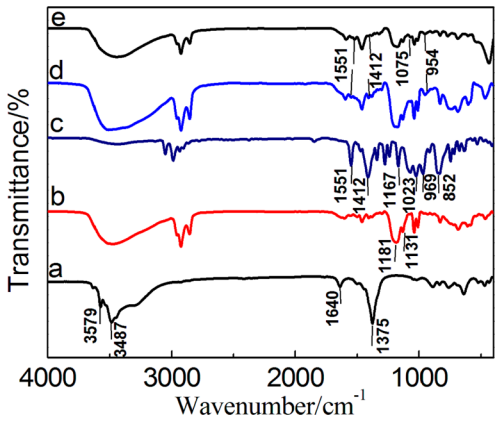

Figure 5. FT-IR spectra of ZHN (a), ZHN−DBS (b), CPF (c), ZHN−DBS−CPF (d), and ZHN−TX-10−CPF (e).

3.1.3. Composition Analysis. Chemical compositions of ZHN−DBS, ZHN−DBS−CPF (1.2, 1.0), ZHN−TX-10−CPF (1.2, 1.0), and ZHN−DB−CPF (1.2, 1.0) are listed in Table 1.The weight percent of Zn has a little change more or less compared to the pristine ZHN−DBS. The CPF loading of ZHN−DBS−CPF (1.2, 1.0), ZHN−TX-10−CPF (1.2, 1.0), and ZHN−DB−CPF (1.2, 1.0) by UV−vis analysis are about 5.7, 16.2 and 46.3%, respectively, which are higher than that in the reference.[29] The CPF loading measured by ion chromatography is lower than that by UV−vis due to the difference methods. However, both results reveal that the CPF loadings decrease in the sequence of ZHN−DB−CPF > ZHN−TX-10−CPF > ZHN−DBS−CPF.

Table 1. Chemical Analysis Data of ZHN−DBS, ZHN−DBS−CPF, ZHN−TX-10−CPF, and ZHN−DB−CPF

	weight percent (%)					CPF loading (%)	
samples	Zn	C	N	H	Cl	U^a	I^a
ZHN−TX-10−CPF	52.70	16.04	1.97	2.78	3.28	16.2	10.81
ZHN−DBS−CPF	42.72	24.78	1.69	4.71	0.60	5.70	1.98
ZHN−DB−CPF	41.21	20.25	3.26	3.38	9.74	43.6	31.22
ZHN−DBS	45.39	30.85	0	8.14			

^{a}*U* and *I* denote the data measured by UV−vis and ion chromatography methods, respectively.

The loadings might be governed by some factors including surface charge density, unoccupied interlayer space, interaction strength between surfactant and the layer, the polarity of gust species,[43,44] physicochemical properties of surfactant, etc. For surfactants DBS, TX-10 and DB, their molecular weights are 348, 660, 271, and the critical micelle concentrations (CMC) are 1.0×10^{-3}, 1.12×10^{-4}, 1.4×10^{-3} mol·L^{-1}, respectively. For the same weight surfactant, the micelle concentration of TX-10 is far higher than that of DBS, and CPF solubilization amount in the former system is higher than that in the latter. In addition, there exists the weak repulsive action among TX-10 molecules, which makes the molecules packing tightly. Therefore, ZHN−TX-10−CPF has the much higher CPF loading than ZHN−DBS−CPF. Furthermore, DB easily forms

DOI: 10.1021/acsami.5b01068
ACS Appl. Mater. Interfaces 2015, 7, 11180−11188

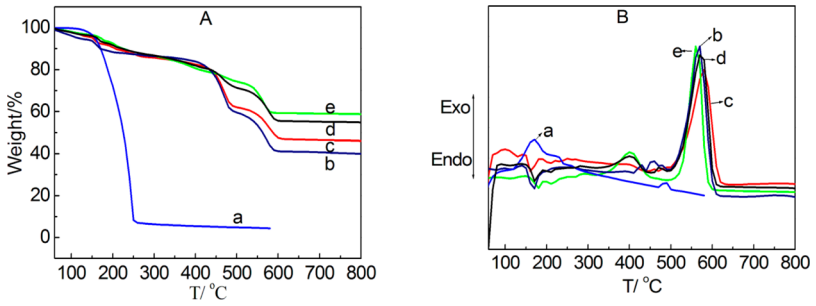

Figure 6. TGA (A) and DTA (B) curves of CPF (a), ZHN−DBS (b), ZHN−DBS−CPF (c), ZHN−TX-10−CPF (d) and ZHN−DBS−CPF-2 (e).

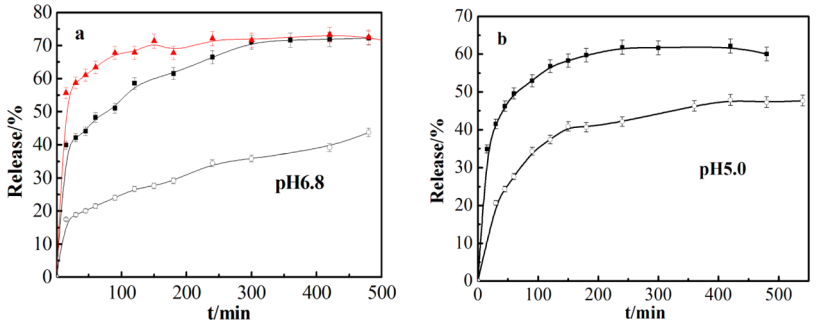

Figure 7. Release profiles for CPF from ZHN−DBS−CPF-2 (▲), ZHN−DBS−CPF (■), and ZHN-TX-10-CPF (*o*) in buffer solutions at pH 6.8 (a) and pH 5.0 (b).

micelles that can solubilize much CPF because of it is a zwitterionic surfactant. And, there exists the strong attractive interactions among DB-CPF micelles, which results into packing tightly of DB and CPF molecules in the gallery, hence ZHN−DB−CPF has the highest CPF loading among three intercalated compounds.

3.1.4. TGA/DTA Analysis. TGA and DTA curves for the pure CPF, ZHN−DBS, ZHN−DBS−CPF, ZHN−TX-10−CPF and ZHN−DBS−CPF-2 are shown in Figure 6A and 6B, respectively. The CPF exhibits two weight loss events (Figure 6A-a). The first event (40−90 °C) is attributed to the melting of CPF. The second event (120−260 °C) is due to the gasification, decomposition and combustion of CPF, with the corresponding exothermic peaks located at 170 and 220 °C in the DTA curve (Figure 6B-a). The ZHN−DBS exhibits three weight loss stages. The first (140−190 °C) corresponds to the removal of surface water and structural water, corresponding to an endothermic peak at 170 °C (Figure 6B-b). The second (390−480 °C) is a consequence of the decomposition of DBS, companying a weak exothermic peak at 460 °C. The third (480−620 °C) is attributed to the combustion of DBS, with a very strong exothermic peak (570 °C). The thermal decomposition of ZHN−DBS−CPF is characterized by four steps: the first (100−180 °C) is due to the loss of the adsorbed and structural water, and the melting of CPF; the second (360−440 °C) is a consequence of CPF combustion, companying a visible exothermic peak at 400 °C (Figure 6B-c); the third (440−470 °C) is a consequence of DBS decomposition; and the fourth (470−620 °C) attributes to the combustion of DBS, with a very strong exothermic peak (580 °C). ZHN−TX-10−CPF also exhibits four weight loss stages like ZHN−DBS−CPF. A distinct exothermic peak appears at 400 °C, which should be attributed to the decomposition and combustion of CPF. And a strong exothermic peak (570 °C) belongs to combustion of TX-10. ZHN−DBS−CPF-2 has the weight loss stages like ZHN−TX-10−CPF. ZHN−DB−CPF also exhibits four weight loss stages like ZHN−TX-10−CPF in Supporting Information Figure S4. The decomposition and combustion of DB corresponds to two exothermic peaks at 550 and 730 °C, which is much higher than that of pure DB (280 and 630 °C). It can be seen that the intercalated CPF has a decomposition temperature about 180 °C higher than the pure (220 °C), showing a higher thermal stability. It also indicates that CPF are successfully intercalated in the gallery. Moreover, the exothermic peak intensity at 400 °C decreases in the sequence of ZHN−DB−CPF > ZHN−TX-10−CPF > ZHN−DBS−CPF, which is in good agreement with the trend of CPF loading amounts in the former section.

3.2. Release of CPF from ZHN−DBS−CPF, ZHN−TX-10−CPF, and ZHN−DB−CPF. The CPF release behaviors of ZHN−DBS−CPF, ZHN−TX-10−CPF, and ZHN−DBS−CPF-2 at pH 6.8 buffer solution are investigated and displayed in Figure 7a. For ZHN−DBS−CPF-2, a rapid release is found within 15 min at the initial, followed by a slow release, and the release equilibrium is reached in about 150 min. In detail, for ZHN−DBS−CPF-2, the $t_{0.5}$ (the time for release fraction of 50%) is 15 min and ∼71% CPF released in 150 min. For ZHN−DBS−CPF, the $t_{0.5}$ is 90 min, and ∼72% CPF released in 360 min. For ZHN−TX-10−CPF, the accumulated release amount is about 44% among the time investigated. It is obvious that CPF release from ZHN−TX-10−CPF and ZHN−DBS−CPF are much slower than that of ZHN−DBS−CPF-2, especially for ZHN−TX-10−CPF. Figure 7 b displays the release behavior of ZHN−DBS−CPF and ZHN−TX-10−CPF at pH 5.0 buffer solution, respectively. For ZHN−DBS−CPF, the $t_{0.5}$ is 60 min and ∼62% CPF released in 240 min. Compared to Figure 7a, the CPF release from ZHN−DBS−CPF at pH 5.0 buffer solution is faster than that at pH 6.8, which may be due to the different release mechanism of CPF.[31] At pH 5.0, ZHN may be dissolved. The release process includes

DOI: 10.1021/acsami.5b01068
ACS Appl. Mater. Interfaces 2015, 7, 11180−11188

the removal of the layers, ion exchange and diffusion in the gallery. At pH 6.8, ZHN should be more stable, and as a result, release process occurs primarily through ion exchange and diffusion. CPF releases from ZHN−TX-10−CPF are much slower than those from ZHN−DBS−CPF at both pH 5.0 and pH 6.8. TX-10 molecules will bring some negative charges due to the hydration. There exists the strong interaction between TX-10 and the layer due to the formation of hydrogen bonding between EO groups and the hydroxyl of layer. Moreover, the weak repulsive actions exist among TX-10 molecules, which make TX-10 difficult to release from the intercalated compounds to the buffer solution. However, for ZHN−DBS−CPF, there exists strong electrostatic repulsive force among DBS anions, which leads to quick desorption of DBS from the layer and diffusion into the buffer solution through ion exchange. Therefore, ZHN−TX-10−CPF exhibits the slower release behavior than ZHN−DBS−CPF.

Furthermore, CPF release from ZHN−DB−CPF at pH 6.8 buffer solution is investigated (Supporting Information Figure S5). A rapid release is found within 15 min at the initial stage, and the release equilibrium is reached in about 90 min. Compared to ZHN−DBS−CPF and ZHN−TX-10−CPF, ZHN−DB−CPF has the fastest CPF release rate, which is due to very weak interaction between DB ions and the layer. In addition, the CPF release from intercalated compounds is not totally complete within 500 min. The partial release may be due to that CPF molecules are deeply embedded in the interlayer and the whole release needs much longer times. This indicates that ZHN−DBS−CPF and ZHN−TX-10−CPF may be used as a potential pesticide controlled release system.

3.3. Release Kinetics of CPF from ZHN−DBS−CPF and ZHN−TX-10−CPF. The release data are fitted by the first-order, pseudo-second-order and parabolic diffusion models, and the fitted plots are displayed in Figure 8. Table 2 also appends the fitted results of rate constants (k) and correlation coefficient (R^2). It is found that the release data are well fitted by pseudo second-order kinetic model and parabolic diffusion model with $R^2 > 0.971$. The similar release behavior has also been found in

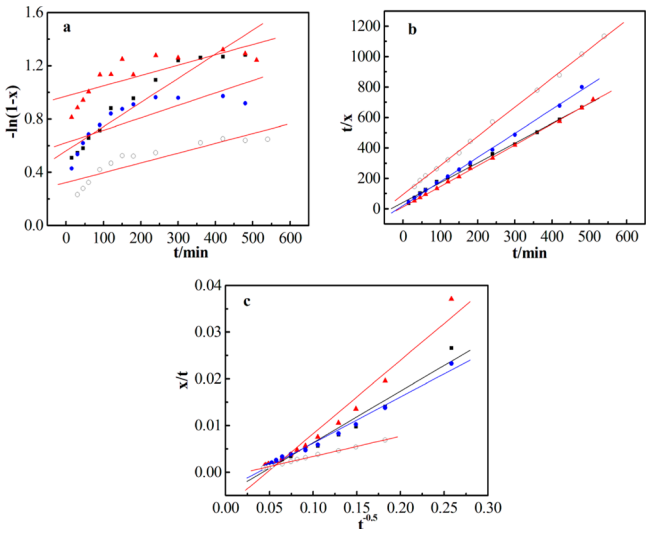

Figure 8. Plots of kinetic equation of (a) first-order model, (b) pseudo-second-order model, and (c) parabolic diffusion model for the release of CPF from the ZHN−DBS−CPF (■) and ZHN−DBS−CPF-2 (▲) at pH 6.8 buffer solution and ZHN−DBS−CPF (●) and ZHN−TX-10−CPF (○) at pH 5.0 buffer solution.

Table 2. Fitted Results of Rate Constants (k) and Correlation Coefficient (R^2) by Three Models

	first-order model		pseudo-second-order model		parabolic diffusion model	
samples[a]	k (10^{-3})	R^2	k	R^2	k	R^2
①	1.8	0.920	1.01	0.998	0.021	0.981
②	0.7	0.979	0.35	0.971	0.048	0.989
③	0.8	0.643	2.06	0.999	0.16	0.982
④	0.9	0.787	2.03	0.999	0.10	0.994
⑤	0.7	0.800	0.27	0.999	0.043	0.999

[a]①, ②, and ③ denote the ZHN−DBS−CPF, ZHN−TX-10−CPF, and ZHN−DBS−CPF-2 at pH 6.8 buffer solution, respectively; ④ and ⑤ denote the ZHN−DBS−CPF and ZHN−TX-10−CPF at pH 5.0 buffer solution, respectively.

the camptothecin from drug−LDH composite.[45] The fitting data from the pseudo-second-order and parabolic diffusion model imply that the release process is controlled by a diffusion process such as intraparticle diffusion between ZHN layers or surface diffusion. Additionally, it is found that the release percent for ZHN−DBS−CPF at pH 6.8 is more than that at pH 5.0. As the pesticide release is due to the diffusion, once the molecules diffuse through the ZHN particle and then the diffusion layer. Thus, the pesticide release could be controlled by the diffusion through the ZHN particle, or by the diffusion through the solution layer surrounding the particle. The release rate of guest molecules would be determined by the slower step of these two processes.[46] For a particle diffusion-controlled release, Bhaskar et al.[47] suggests that particle diffusion control can be simply tested by linearity between $\ln(1 - x_t)$ verus $t^{0.65}$. A good linear relationship (correlation coefficient = 0.981) is obtained for ZHN−DBS−CPF at pH 6.8, while at pH 5.0 such a line cannot be obtained, indicating that diffusion through the ZHN particle is the rate limiting step for ZHN−DBS−CPF at pH 6.8. The similar phenomenon has also been observed by Liu et al.[46]

4. CONCLUSIONS

CPF encapsulation into the gallery of ZHN is successfully achieved with the aid of CPF micelles into ZHN−DBS. The basal spacings of ZHN−DBS−CPF, ZHN−TX-10−CPF, and ZHN−DB−CPF are 3.29−3.59, 2.57−2.87, and 1.97 nm, respectively, which indicate that the different intercalation mechanisms exist among them. For ZHN−DBS−CPF, CPF adsolubilization into the galleries is well achieved by the second intercalation of DBS-CPF micelles into the enlarged gallery of ZHN−DBS; for ZHN−TX-10−CPF, CPF intercalation into the galleries is completed by the exchange of TX-10-CPF micelles with the intercalated DBS; for ZHN−DB−CPF, the intercalated DBS is induced and removed due to the strong interaction between DB and DBS anions, and the other DB accompanying CPF enter into the gallery. The CPF loading amounts increases in the sequence of ZHN−DBS−CPF < ZHN−TX-10−CPF < ZHN−DB−CPF. The combustion temperature of the intercalated CPF increases to 400 °C from 220 °C for the isolated, indicating CPF stability are greatly improved, which further confirms that CPF are successfully incorporated in the gallery.

CPF releases behaviors of ZHN−DBS−CPF (ZHN−TX-10−CPF, ZHN−DB−CPF) rely on surfactant type and release environments. ZHN−DBS−CPF (ZHN−TX-10−CPF) has the faster CPF release at pH 5.0 than pH 6.8 buffer solutions,

DOI: 10.1021/acsami.5b01068
ACS Appl. Mater. Interfaces 2015, 7, 11180−11188

which is due to the process including the removal of ZHN layers, ion exchange and diffusion of CPF. CPF release from ZHN−TX-10−CPF is much slower than that from ZHN−DBS−CPF, which is caused from the strong interaction between TX-10 molecules and the layer. However, ZHN−DB−CPF has the fastest release rate among them due to the very weak interaction between DB and the layer. Furthermore, release data of ZHN−DBS−CPF and ZHN−TX-10−CPF are well fitted by pseudo-second-order and parabolic diffusion models. The present results suggest that this method could broaden the application of surfactants, and ZHN−DBS−CPF and ZHN−TX-10−CPF could be potentially used as a novel controlled-release formulation of the pesticide.

■ ASSOCIATED CONTENT

Supporting Information

XRD patterns of ZHN−DBS prepared at different pH values and temperatures, XRD patterns of ZHN−DB−CPF (1.2, 1.0) samples, FT-IR spectra of ZHN−DB−CPF, TGA and DTA curves of DB, ZHN−DB−CPF, release profiles for CPF from ZHN−DB−CPF in pH 6.8 buffer solutions. The Supporting Information is available free of charge on the ACS Publications website at DOI: 10.1021/acsami.5b01068.

■ AUTHOR INFORMATION

Corresponding Author

*E-mail: xgzhang@nankai.edu.cn.Tel: +86 22 23499474.

Notes

The authors declare no competing financial interest.

■ ACKNOWLEDGMENTS

We are grateful for Colleges and Universities of Hebei Province Science and Technology Research Projects, China (QN20131050), Natural Science Foundation of Hebei Province, China (B2015202046), and Key Laboratory of Colloid and Interface Chemistry, Ministry of Education, Shandong University (201202).

■ REFERENCES

(1) Arízaga, G. G. C.; Satyanarayana, K. G.; Wypych, F. Layered Hydroxide Salts: Synthesis, Properties and Potential Applications. *Solid State Ionics* **2007**, *178*, 1143−1162.

(2) Vaccari, A. Preparation and Catalytic Properties of Cationic and Anionic Clays. *Catal. Today* **1998**, *41*, 53−71.

(3) Poznyak, S. K.; Tedim, J.; Rodrigues, L. M.; Salak, A. N.; Zheludkevich, M. L.; Dick, L. F. P.; Ferreira, M. G. S. Novel Inorganic Host Layered Double Hydroxides Intercalated with Guest Organic Inhibitors for Anticorrosion Applications. *ACS Appl. Mater. Interfaces* **2009**, *1*, 2353−2362.

(4) Kang, N. J.; Wang, D. Y.; Kutlu, B.; Zhao, P. C.; Leuteritz, A.; Wagenknecht, U.; Heinrich, G. A New Approach to Reducing the Flammability of Layered Double Hydroxide (LDH)-Based Polymer Composites: Preparation and Characterization of Dye Structure-Intercalated LDH and Its Effect on the Flammability of Polypropylene-Grafted Maleic Anhydride/D-LDH Composites. *ACS Appl. Mater. Interfaces* **2013**, *5*, 8991−8997.

(5) Jiang, S. D.; Bai, Z. M.; Tang, G.; Song, L.; Stec, A. A.; Hull, T. R.; Hu, Y.; Hu, W. Z. Synthesis of Mesoporous Silica@Co-Al Layered Double Hydroxide Spheres: Layer-by-Layer Method and Their Effects on the Flame Retardancy of Epoxy Resins. *ACS Appl. Mater. Interfaces* **2014**, *6*, 14076−14086.

(6) Bull, R. M. R.; Markland, C.; Williams, G. R.; O'Hare, D. Hydroxy Double Salts as Versatile Storage and Delivery Matrices. *J. Mater. Chem.* **2011**, *21*, 1822−1828.

(7) Oh, J. M.; Biswick, T. T.; Choy, J. H. Layered Nanomaterials for Green Materials. *J. Mater. Chem.* **2009**, *19*, 2553−2563.

(8) Bi, X.; Fan, T.; Zhang, H. Novel Morphology-Controlled Hierarchical Core@Shell Structural Organo-Layered Double Hydroxides Magnetic Nanovehicles for Drug Release. *ACS Appl. Mater. Interfaces* **2014**, *6*, 20498−20509.

(9) Li, F.; Jin, L.; Han, J.; Wei, M.; Li, C. Synthesis and Controlled Release Properties of Prednisone Intercalated Mg−Al Layered Double Hydroxide Composite. *Ind. Eng. Chem. Res.* **2009**, *48*, 5590−5597.

(10) Liu, J. X.; Zhang, Y. Q.; Zhang, X. G.; Wang, J. L.; Zhao, L. F.; Yang, J.; Wang, R. Preparation and Characterization of Intercalation Materials with Layered Hydroxide Salts (LHS). *Chin. J. Inorg. Chem.* **2014**, *30*, 837−844.

(11) Yang, J. H.; Han, Y. S.; Park, M.; Park, T.; Hwang, S. J.; Choy, J. H. New Inorganic-Based Drug Delivery System of Indole-3-Acetic Acid-Layered Metal Hydroxide Nanohybrids with Controlled Release Rate. *Chem. Mater.* **2007**, *19*, 2679−2685.

(12) Marangoni, R.; Mikowski, A.; Wypych, F. Effect of Adsorbed/Intercalated Anionic Dyes into the Mechanical Properties of PVA: Layered Zinc Hydroxide Nnitrate Nanocomposites. *J. Colloid Interface Sci.* **2010**, *351*, 384−391.

(13) Cursino, A. C. T.; da Costa Gardolinski, J. E. F.; Wypych, F. Intercalation of Anionic Organic Ultraviolet Ray Absorbers into Layered Zinc Hydroxide Nitrate. *J. Colloid Interface Sci.* **2010**, *347*, 49−55.

(14) Costantino, U.; Ambrogi, V.; Nocchetti, M.; Perioli, L. Hydrotalcite-like Compounds: Versatile Layered Hosts of Molecular Anions with Biological Activity. *Microporous Mesoporous Mater.* **2008**, *107*, 149−160.

(15) Ghotbi, M. Y.; Bagheri, N.; Sadrnezhaad, S. K. Zinc-Stearate-Layered Hydroxide Nanohybrid Material as a Precursor to Produce Carbon Nanoparticles. *J. Alloys Compd.* **2011**, *509*, 2441−2444.

(16) Demel, J.; Pleštil, J.; Bezdička, P.; Janda, P.; Klementova, M.; Lang, K. Layered Zinc Hydroxide Salts: Delamination, Preferred Orientation of Hydroxide Lamellae, and Formation of ZnO Nanodiscs. *J. Colloid Interface Sci.* **2011**, *360*, 532−539.

(17) Arízaga, G. G. C.; da Costa Gardolinski, J. E. F.; Schreiner, W. H.; Wypych, F. Intercalation of an Oxalatooxoniobate Complex into Layered Double Hydroxide and Layered Zinc Hydroxide Nitrate. *J. Colloid Interface Sci.* **2009**, *330*, 352−358.

(18) Arízaga, G. G. C.; Mangrich, A. S.; Gardolinski, J. E. F. C.; Wypych, F. Chemical Modification of Zinc Hydroxide Nitrate and Zn−Al-layered Double Hydroxide with Dicarboxylic Acids. *J. Colloid Interface Sci.* **2008**, *320*, 168−176.

(19) Arízaga, G. G. C. Intercalation Studies of Zinc Hydroxide Chloride: Ammonia and Amino Acids. *J. Solid State Chem.* **2012**, *185*, 150−155.

(20) Biswick, T.; Park, D. H.; Choy, J. H. Enhancing the UV A1 Screening Ability of Caffeic Acid by Encapsulation in Layered Basic Zinc Hydroxide Matrix. *J. Phys. Chem. Solid.* **2012**, *73*, 1510−1513.

(21) Biswick, T.; Park, D. H.; Shul, Y. G.; Choy, J. H. P-coumaric Acid−Zinc Basic Salt Nanohybrid for Controlled Release and Sustained Antioxidant Activity. *J. Phys. Chem. Solids.* **2010**, *71*, 647−649.

(22) Lea, D.; Malha, B. B.; Peggy, R.; Joell, C.; Philippe, L.; Laurent, C.; Fabrice, L.; Christine, T. G.; Bruno, P. Self-Assembly and Characterization of Layered Double Hydroxide/DNA Hybrids. *Nano Lett.* **2006**, *6*, 199−204.

(23) Costantino, U.; Coletti, N.; Nocchetti, M. Anion Exchange of Methyl Orange into Zn−Al Synthetic Hydrotalcite and Photophysical Characterization of the Intercalates Obtained. *Langmuir* **1999**, *15*, 4454−4460.

(24) Nakayama, H.; Wada, N.; Tsuhako, M. Intercalation of Amino Acids and Peptides into Mg−Al Layered Double Hydroxides by Reconstruction Method. *Int. J. Pharm.* **2004**, *269*, 469−478.

(25) Dékáany, I.; Berger, F.; Imrik, K.; Lagaly, G. Hydrophobic Layered Double Hydroxides (LDHs): Selective Adsorbents for Liquid Mixtures. *Colloid Polym.* **1997**, *275*, 681−688.

DOI: 10.1021/acsami.5b01068
ACS Appl. Mater. Interfaces 2015, 7, 11180−11188

(26) Pavan, P. C.; Crepaldi, E. L.; Ǵomez, G.; Valim. Adsorption of Sodium Dodecylsulfate on a Hydrotalcite-like Compound. Effect of Temperature, pH, and Ionic strength. *J. Colloids Surf. A* **1999**, *154*, 399−410.
(27) Morioka, H.; Tagaya, H.; Karasu, M.; Kadokawa, J.; Chiba, K. Preparation of New Useful Materials by Surface Modification of Inorganic Layered Compound. *J. Solid State Chem.* **1995**, *117*, 337−342.
(28) Hou, W. G.; Jin, Z. L. Synthesis and Characterization of Naproxen Intercalated Zn−Al Layered Double Hydroxides. *Colloid Polym. Sci.* **2007**, *285*, 1449−1454.
(29) Wang, B.; Zhang, H.; Evans, D. G.; Duan, X. Surface Modification of Layered Double Hydroxides and Incorporation of Hydrophobic Organic Compounds. *Mater. Chem. Phys.* **2005**, *92*, 190−196.
(30) You, Y. W.; Zhao, H. T.; Vance, G. F. Surfactant-Enhanced Adsorption of Organic Compounds by Layered Double Hydroxides. *Colloids Surf., A* **2002**, *205*, 161−172.
(31) Tyner, K. M.; Schiffman, S. R.; Giannelis, E. P. Nanobiohybrids as Delivery Vehicles for Camptothecin. *J. Controlled Release* **2004**, *95*, 501−514.
(32) Quan, Z. L.; Yang, H.; Zheng, B.; Hou, W. G. Synthesis and Release Behavior of Bactericides Intercalated Mg−Al Layered Double Hydroxides. *Colloids Surf., A* **2009**, *348*, 164−169.
(33) Marangoni, R.; Ramos, L. P.; Wypych, F. New Multifunctional Materials Obtained by the Intercalation of Anionic Dyes into Layered Zinc Hydroxide Nitrate Followed by Dispersion into Poly(Vinyl Alcohol) (PVA). *J. Colloid Interface Sci.* **2009**, *330*, 303−309.
(34) Zhang, H.; Pan, D.; Zou, K.; He, J.; Duan, X. A Novel Core−Shell Structured Magnetic Organic−Inorganic Nanohybrid Involving Drug-Intercalated Layered Double Hydroxides Coated on a Magnesium Ferrite Core for Magnetically Controlled Drug Release. *J. Mater. Chem.* **2009**, *19*, 3069−3077.
(35) Jiang, W.; Su, H. J.; Huo, H. Y.; Tan, T. W. Synthesis and Properties of Surface Molecular Imprinting Adsorbent for Removal of Pb^{2+}. *Appl. Biochem. Biotechnol.* **2010**, *160*, 467−476.
(36) bin Hussein, M. Z.; Ghotbi, M. Y.; Yahaya, A. H.; Rahman, M. Z. A. The effect of polymers onto the size of zinc layered hydroxide salt and its calcined product. *Solid State Sci.* **2009**, *11*, 368−375.
(37) Biswick, T.; Park, D. H.; Shul, Y. G.; Choy, J. H. P-Coumaric Acid−Zinc Basic Salt Nanohybrid for Controlled Release and Sustained Antioxidant Activity. *J. Phys. Chem. Solids.* **2010**, *71*, 647−649.
(38) Newman, S. P.; Jones, W. Comparative Study of Some Layered Hydroxide Salts Containing Exchangeable Interlayer Anions. *J. Solid State Chem.* **1999**, *148*, 26−40.
(39) Cursino, A. C. T.; Lisboa, F. D. S.; Pyrrho, A. D. S.; de Sousa, V. P.; Wypych, F. Layered Double Hydroxides Intercalated with Anionic Surfactants/Benzophenone as Potential Materials for Sunscreens. *J. Colloid Interface Sci.* **2013**, *397*, 88−95.
(40) Cen, G. Q. *Micellization and Synergistic Effects in Mixed Anionic/Nonionic Surfactant Systems [D]*; Hainan University: Haikou, China, 2012.
(41) Islam, M. R.; Guo, Z. H.; Rutman, D.; Benson, T. J. Immobilization of Triazabicyclodecene in Surfactant Modified Mg/Al Layered Double Hydroxides. *RSC Adv.* **2013**, *3*, 24247−24255.
(42) Zhang, Z. Q.; Xu, G. Y.; Ye, F.; Zheng, L. Q.; Luan, Y. X. Surface Activity of Mixed System of Dodecyl Betaine and Sodium Dodecyl Sulphate. *Acta. Phys. Chem. Sin.* **2001**, *17* (12), 1122−1125.
(43) Khan, M. A.; Choi, C. L.; Lee, D. H.; Park, M.; Lim, B. K.; Lee, J. Y.; Choi, J. Synthesis and Properties of Mecoprop-Intercalated Layered Double Hydroxide. *J. Phys. Chem. Solids.* **2007**, *68*, 1591−1597.
(44) Celis, R.; Hermosin, M. C.; Carrizosa, M. J.; Cornejo, J. Inorganic and Organic Clays as Carriers for Controlled Release of the Herbicide Hexazinone. *J. Agric. Food Chem.* **2002**, *50*, 2324−2330.
(45) Dong, L.; Li, Y.; Hou, W. G.; Liu, S. J. Synthesis and Release Behavior of Composites of Camptothecin and Layered Double Hydroxide. *J. Solid State Chem.* **2010**, *183*, 1811−1816.
(46) Liu, C. X.; Hou, W. G.; Li, L. F.; Li, Y.; Liu, S. J. Synthesis and Characterization of 5-Fluorocytosine Intercalated Zn−Al Layered Double Hydroxide. *J. Solid State Chem.* **2008**, *181*, 1792−1797.
(47) Bhaskar, R.; Murthy, S. R. S.; Miglani, B. D.; Viswanathan, K. Novel Method to Evaluate Diffusion Controlled Release of Drug from Resinate. *Int. J. Pharm.* **1986**, *28*, 59−66.

DOI: 10.1021/acsami.5b01068
ACS Appl. Mater. Interfaces 2015, 7, 11180−11188